TDA Progress Report 42-99

November 15, 1989

Disturbance Torque Rejection Properties of the NASA/JPL 70-Meter Antenna Axis Servos

R. E. Hill
Ground Antenna and Facilities Engineering Section

Analytic methods for evaluating pointing errors caused by external disturbance torques are developed and applied to determine the effects of representative values of wind and friction torques. The expressions relating pointing errors to disturbance torques are shown to be strongly dependent upon the state estimator parameters, as well as upon the state feedback gain and the flow-versus-pressure characteristics of the hydraulic system. Under certain conditions, when control is derived from an uncorrected estimate of integral position error, the desired Type II servo properties are not realized and finite steady-state position errors result. Methods for reducing these errors to negligible proportions through the proper selection of control gain and estimator correction parameters are demonstrated. The steady-state error produced by a disturbance torque is found to be directly proportional to the hydraulic internal leakage. This property can be exploited to provide a convenient method of determining system leakage from field measurements of estimator error, axis rate, and hydraulic differential pressure.

I. Introduction

Recent studies of mechanisms contributing to limit-cycle behavior have led to a need for more accurate modeling of the disturbance torque response characteristics of the 70-m antenna axis servos. Of particular interest in the limit-cycle studies is the transient behavior of the various plant and estimator states that occur during friction-induced limit cycling. The traditional assumption that the estimator states accurately track those of the plant becomes inaccurate when the plant is subjected to external disturbance torques. This shortcoming necessitated the development of the present multivariable axis servo model where the plant and estimator states are distinct.

Precise pointing of the 70-m antenna is accomplished through the use of a two-axis, azimuth-elevation, bullgear-driven servo system. Control torques are produced by fixed-displacement, axial-piston hydraulic motors, which are coupled to the axis bullgears through spur-gear reducers. Four such motor/gear reducers are employed for each axis. Backlash is eliminated by separate countertorque motors which apply a constant torque bias to the output pinion of each control motor. The hydraulic connections to the countertorque motors are arranged as shown in Fig. 1 so as to preload all four gear reducers and apply zero net torque to the bullgear. Torque modulation is accomplished by four port-hydraulic servo valves. Servo control consists of a hardware rate loop with tachometer feedback and a computer-based position servo employing state-variable feedback.

The servo model is based on the nonlinear orifice-flow equation of the valve, along with the motor-flow equation

as described in [1]. A piecewise linear representation of the valve is obtained by partial differentiation of the valve equation (Eq. 5 of [1]) to yield the flow Q_v as a linear function of the valve input current I_v and load pressure P_L:

$$Q_v = K_P I_v - D_H P_L \tag{1}$$

with

$$K_P = K_v P_v^{1/2}$$

$$D_H = \frac{Q_v}{P_v}$$

and

$$P_v = P_S - P_L - P_R$$

where P_S and P_R are the regulated system supply pressure and return pressure, respectively. As shown later, the load pressure is sufficiently small relative to the supply pressure such that the range of the valve pressure remains within a 2 to 1 ratio. This justifies the use of a constant value approximation for the flow gain K_P for control dynamic analysis. In contrast, the equivalent damping D_H is linearly proportional to the flow, which varies in proportion to antenna rate. Therefore, D_H varies between a minimum value corresponding to leakage flow at the zero antenna rate, and a maximum corresponding to the maximum tracking rate of the antenna.

The hydromechanical system model incorporates the linearized valve of Eq. (1) along with a motor coupled to a rigid-body inertia load representation of the antenna structure, as shown in block diagram form in Fig. 2, where C_H, J_M, and V_M represent the hydraulic compressibility, motor inertia, and motor displacement, respectively.

The block diagram of the equivalent plant (servo-loop hardware) in Fig. 3 incorporates the model of Fig. 2, the tachometer feedback and control amplifier with associated compensation networks, and two additional integrations which produce the angular position and position integral states. The two inputs represent the electrical rate command input to the plant and an equivalent external disturbance torque; K_R represents a constant with value proportional to the rate loop gain, and P_2 and Z_2 are the pole and zero frequencies of the rate loop compensation network. Figure 3 also includes a simplified equivalent of the tachometer feedback network obtained by neglecting the network pole, which is at a relatively high frequency. This approximation introduces the acceleration feedback branch shown in Fig. 3 where the parameter Z_1 corresponds to the negative real frequency of the network zero.

To provide additional insight into the effects of rate and position loop parameters on system compliance, compliance equations are developed separately for the open-position loop case, for the hardware position proportional, integral, and derivative (PID) feedback, and for the closed-loop state variable controller. It is shown that the combination of plant-state and estimator-state feedback in the precision mode leads to compliance characteristics different from those of the computer mode, even when both modes have identical plant and estimator dynamics.

II. Compliance Equations for the Open Position Loop Case

The open position loop compliance can be derived from the angular position response to a unit-step torque input. By application of the Mason transmittance rule to the block diagram of Fig. 3, the compliance transfer function becomes:

$$\frac{\Theta_M}{T_X} = \frac{(1/J_M s^2)(1 + D_H/C_H s)(1 + P_2/s)}{(1 + P_2/s)(1 + D_H/C_H s + K_R/C_H J_M Z_1 s + (V_M^2 + K_R)/J_M C_H s^2) + (Z_2 - P_2)(K_R/C_H J_M s^2)(1/s + 1/Z_1)}$$

which leads to

$$\frac{\Theta_M}{T_X} = \frac{(1/s)(s + D_H/C_H)(s + P_2)}{J_M(s + P_2)(s^2 + (D_H/C_H)s + V_M^2/J_M C_H) + (K_R/C_H Z_1)(s + Z_1)(s + Z_2)} \tag{2}$$

Application of the final value theorem to Eq. (2) indicates a constant steady-state rate in response to a step function torque disturbance. The steady-state compliance is given by

$$\frac{\Theta_M}{T_X} = \frac{D_H}{s(V_M^2 + K_R Z_2/P_2)}$$

III. Compliance Equations for Hardware PID Feedback

The compliance of the closed-loop PID feedback system can be calculated by the same method used earlier for the open-loop case. The addition of position, integral, and rate feedback branches produces three additional denominator terms in the compliance expressions. Thus,

$$\begin{aligned}\frac{\Theta_M}{T_X} = \frac{(1/J_M s^2)(1 + D_H/C_H s)(1 + P_2/s)}{(1 + P_2/s)(1 + D_H/C_H s + K_R/C_H J_M Z_1 s + (V_M^2 + K_R)/J_M C_H s^2)} \\ + (Z_2 - P_2)(K_R/C_H J_M s^2)(1/s + 1/Z_1 + K_1/s^3 + K_2/s^2 + K_3/s) \\ + (1 + P_2/s)(K_R/C_H J_M s)(K_1/s^3 + K_2/s^2 + K_3/s)\end{aligned}$$

which leads to

$$\begin{aligned}\frac{\Theta_M}{T_X} = \frac{s(s + D_H/C_H)(s + P_2)}{J_M s^2(s + P_2)(s^2 + (D_H/C_H)s + V_M^2/J_M C_H)} \\ +(K_R/C_H)(s + Z_2)(s^2 + s^3/Z_1 + K_1 + K_2 s + K_3 s^2)\end{aligned} \tag{3}$$

and the steady-state compliance becomes

$$\frac{\Theta_M}{T_X} = \frac{D_H s}{K_1 K_R (Z_2/P_2)}$$

The compliance transfer functions of Eqs. (2) and (3) include numerator zeros corresponding to the network pole P_2 and to the effective hydraulic damping D_H/C_H. The denominators are seen to contain the poles of the respective open/closed-loop system. From the dependence of D_H on hydraulic flow, the steady-state compliance properties are seen to be antenna-rate dependent. For typical closed-position loop parameter values, the damping D_H has relatively little effect on the closed-loop poles. Therefore, since the shape of the compliance transient is determined by the locations of the transfer function zeros relative to the poles, the closed-loop transient properties are also seen to vary as a function of D_H.

IV. Compliance Equations for the State Variable Controller

Earlier methods of disturbance torque effects analysis [2] were based on the assumption of negligible errors in the estimator states in relation to the corresponding plant states. This permitted a simplification of the system model by substituting plant-state feedback in place of the estimator-state feedback, thereby reducing the number of states required in the model. This assumption, widely used in evaluating command input transient responses, was found to produce finite errors in the determination of disturbance transient responses of the axis servos. It was subsequently replaced by a superior method employing full modeling of the estimator states as well as the plant states.

The model for disturbance torque response of the state-variable axis servo controller is based on a linearized multi-input state-variable representation of the system of Fig. 3, with the addition of the state-estimator and control-feedback gain. The plant state is represented by the generalized state equations, where $\dot{x}$ and Y are the state and output by

$$\dot{x} = \mathbf{A}x + \mathbf{B}U$$

$$Y = \mathbf{C}x + \mathbf{D}U$$

respectively.

The corresponding **A**, **B**, **C**, **D** matrices from Fig. 3 are:

$$\mathbf{A} = \begin{bmatrix} 0 & 1 & 0 & 0 & 0 \\ 0 & 0 & 1 & 0 & 0 \\ 0 & 0 & 0 & 1J_M & 0 \\ 0 & 0 & -V_M^2/C_H - K_R/C_H & -D_H/C_H - K_R/C_H J_M Z_1 & K_R(Z_2 - P_2)/C_H \\ 0 & 0 & -1 & -1/J_M Z_1 & -P_2 \end{bmatrix}$$

$$\mathbf{B} = \begin{bmatrix} 0 & 0 \\ 0 & 0 \\ 0 & 1/J_M \\ K_R/C_H & -K_R/C_H J_M Z_1 \\ 1 & -1/J_M Z_1 \end{bmatrix}$$

$$\mathbf{C} = \begin{bmatrix} 0 & 1 & 0 & 0 & 0 \end{bmatrix}$$

$$\mathbf{D} = \begin{bmatrix} 0 & 0 \\ 0 & 0 \\ 0 & 0 \\ 0 & 0 \\ 0 & 0 \end{bmatrix}$$

Representing the estimator state by $\hat{x}$, and estimator output by $\hat{Y}$, the estimator equations become:

$$\dot{\hat{x}} = \mathbf{A}\hat{x} + B_1 U_1 + L(Y - \hat{Y})$$

$$\hat{Y} = \mathbf{C}\hat{x} + D_1 U_1$$

where B_1, B_2, D_1, D_2, U_1, and U_2 represent the first and second columns of **B** and **D** and the first and second elements of **U**, respectively. This distinction is essential because both inputs couple directly into the plant, while only the rate command input U_1 couples directly into the estimator.

V. Computer Control Mode

Because the rate command U_1 is formed differently for the precision mode, the two control modes are addressed separately. Incorporating the control-feedback gain K into the expression for the rate command input U_1 for computer mode, and substituting into the plant and estimator equations leads to

$$U_1 = -K\hat{x}$$

$$\dot{x} = \mathbf{A}x - B_1 K\hat{x} + B_2 U_2 \tag{4}$$

$$\dot{\hat{x}} = LCx + (\mathbf{A} - B_1 K - LC - LD_1 K)\hat{x} + LD_2 U_2$$

C-3

With the estimator error,

$$\tilde{x} = x - \hat{x}$$

$$\dot{\tilde{x}} = (\mathbf{A} - LC)\tilde{x} + LD_1K\hat{x} + (B_2 - LD_2)U_2$$

Since for the present case both D_1 and D_2 are zero, the estimator and estimator-error equations simplify to

$$\dot{\hat{x}} = LCx + (\mathbf{A} - B_1K - LC)\hat{x} \tag{5}$$

and

$$\dot{\tilde{x}} = (\mathbf{A} - LC)\tilde{x} + B_2U_2 \tag{6}$$

The equations for the plant and estimator are illustrated in the state-space block diagram in Fig. 4. Combining Eqs. (4) and (5) to form a single state vector comprising the plant and estimator states leads to the matrix differential equation form

$$\begin{bmatrix} \dot{x} \\ \dot{\hat{x}} \end{bmatrix} = \begin{bmatrix} \mathbf{A} & -B_1K \\ LC & \mathbf{A} - B_1K - LC \end{bmatrix} \begin{bmatrix} x \\ \hat{x} \end{bmatrix} + \begin{bmatrix} B_2 \\ 0 \end{bmatrix} U_2 \tag{7}$$

which is compatible with existing linear system analysis and simulation software tools. The steady-state disturbance torque compliance properties of the combined plant and estimator system can be determined from the steady-state solution of Eq. (7). The general expressions for the steady-state values of the individual plant and estimator states can be determined by a symbolic expansion of the determinants resulting from application of Simpson's Rule to Eq. (7).

Since, in the steady state, the derivatives represented by the left-hand side of Eq. (7) equal zero, steady-state position estimate $\hat{x}_2$ becomes

$$\frac{\hat{x}_2}{U_2} = \frac{-\det \left[\begin{array}{c|c|c|c} & & & \\ \mathbf{A} & -B_1k_1 & B_2 & B_1\left[k_3k_4k_5\right] \\ & & & \\ \hline & & 0 & \\ & \mathbf{A}_1 & 0 & \\ LC & -B_1k_1 - LC_1 & 0 & \mathbf{A}_{3,5} - B_1\left[k_3\,k_4\,k_5\right] \\ & & 0 & \\ & & 0 & \end{array}\right]}{\det \begin{bmatrix} \mathbf{A} & -B_1K \\ LC & \mathbf{A} - B_1K - LC \end{bmatrix}} \tag{8}$$

where the numerator matrix is obtained from the 10 × 10 denominator matrix by replacing the column corresponding to $\hat{x}_2$ (column 7) with the right-hand-side vector, in accordance with Simpson's Rule. The subscripts applied to capital-letter symbols designate the respective columns of the associated matrix, and $\mathbf{A}_{3,5}$ denotes a matrix comprised of the third through fifth columns of $\mathbf{A}$.

A row by row examination of the numerator matrix reveals that the sixth row is comprised of the five elements of the first row of LC, a single element $(a_{11} - b_{11}k_1 - l_1c_1)$, and the last three elements of the first row of $[\mathbf{A} - B_1K - LC]$. It will be seen that, since the first element of L is zero in the current parameter set, and because of the sparseness of $\mathbf{A}$ and $\mathbf{B}$, the elements of the sixth row are all zeros and the numerator determinant vanishes. This indicates that, in the presence of a constant disturbance torque, the steady-state position estimate $\hat{x}_2$ is identically equal to zero. This in turn indicates that the final values of the position x_2 and the position estimation error $\tilde{x}_2$ are identical, and x_2 can

thus be evaluated using Eq. (6). This approach avoids the complexity of evaluating the determinant of the 10 × 10 matrices of Eq. (8).

Thus, in the steady state, using Eq. (6),

$$\dot{\tilde{x}} = (\mathbf{A} - LC)\tilde{x} + B_2 U_2 = 0$$

and

$$\tilde{x} = \frac{-\det\begin{bmatrix}\mathbf{A}_1 & B_2 & \mathbf{A}_3 & \mathbf{A}_4 & \mathbf{A}_5\end{bmatrix}}{\det\begin{bmatrix}\mathbf{A} & -LC\end{bmatrix}} U_2$$

Note that L and C are absent from the numerator because all elements of C, except for the second, are zero. Note also that the first row of $\mathbf{A}$ and the first element of C are zero, causing both determinants to vanish. However, since the plant integral state is uncoupled from both the plant and the estimator, the corresponding first rows and columns can be deleted from both the numerator and denominator with no loss in generality. It should be noted that if the first element of C is assigned a nonzero value, the denominator determinant remains finite as long as L is nonzero. The implications of this integral position feedback will be discussed later.

Substituting the values of $\mathbf{A}$, B_2, and C into the expression for $\tilde{x}_2$,

$$\frac{\tilde{x}_2}{U_2} = \frac{\det\begin{bmatrix} 0 & 1 & 0 & 0 \\ -1/J_M & 0 & 1/J_M & 0 \\ K_R/C_H J_M Z_1 & -V_M^2/C_H - K_R/C_H & -D_H/C_H - K_R/C_H J_M Z_1 & K_R(Z_2 - P_2)/C_H \\ 1/J_M Z_1 & -1 & -1/J_M Z_1 & -P_2 \end{bmatrix}}{\det\begin{bmatrix} -l_2 & 10 & 0 & \\ -l_3 & 0 & 1/J_M & 0 \\ -l_4 & -V_M^2/C_H - K_R/C_H & -D_H/C_H - K_R/C_H J_M Z_1 & K_R(Z_2 - P_2)/C_H \\ -l_5 & -1 & -1/J_M Z_1 & -P_2 \end{bmatrix}}$$

Expanding the determinants leads to the nonzero steady-state position estimate error $\tilde{x}_2$, and since the steady-state plant position x_2 equals $\tilde{x}_2$,

$$\frac{x_2}{U_2} = \frac{D_H}{l_2(V_M^2 + K_R Z_2/P_2) + l_3(D_H J_M + K_R Z_2/Z_1 P_2) + l_4 C_H + l_5(Z_2/P_2 - 1)}$$

which, using current 70-m antenna servo parameter values, can be approximated by

$$\frac{x_2}{U_2} \cong \frac{D_H P_2/Z_2}{K_R l_2}$$

This result invalidates the original premise that control feedback of estimated integral error is equivalent to feedback of plant integral error in imparting Type II servo performance. That premise is valid only for inputs, such as the position command, which are coupled equally to the estimator and the plant. From Eqs. (3) and (4) and the block diagram of Fig. 4, it is seen that the plant is influenced by the control input U_1 and a disturbance input U_2, while the estimator is influenced by the same control input and by the estimator feedback error $LC\tilde{x}$. In equilibrium, the plant disturbance U_2 is compensated by the control input U_1; thus, the identical U_1 input to the estimator must be counteracted by the error $LC\tilde{x}$ in order to obtain estimator equilibrium. This implies that a finite estimator error $\tilde{x}$ will always result from a plant disturbance input, while the individual components of $\tilde{x}$ will be determined by the product of L and C. This line of reasoning explains the absence of the control gain K from the steady-state compliance expression.

In the present case, where there is no feedback of x_1, the integral estimate error $\tilde{x}_1$ is allowed to grow unbounded. The addition of a small amount of plant integral feedback to the estimator by assigning a small value to c_1 would bound the error $\tilde{x}_1$, thereby forcing $\tilde{x}_2$, x_2, and $\hat{x}_2$ to zero. The required nonzero $\tilde{x}$ would then result from nonzero values of the components other than $\tilde{x}_2$ and $\tilde{x}_3$. This additional feedback imparts the desired disturbance accommodating control [3] properties to the system.

VI. Precision-Control Mode

In the precision (autocollimator feedback) mode, the control input U_2 is derived from the autocollimator, an electro-optical device that senses plant position error directly. This error signal is filtered to remove noise and then integrated. The resulting plant integral and position errors are then combined with additional damping terms provided by the position estimate to form the plant input according to

$$U_1 = -k_1 x_1 - k_2 x_2 - k_3 \hat{x}_3 - k_3 \hat{x}_4 - k_5 \hat{x}5$$

The resulting system equations therefore take a slightly different form from that of Eq. (7) due to the mixed plant and estimator feedback. Thus, for precision mode,

$$\begin{bmatrix} \dot{x} \\ \dot{\hat{x}} \end{bmatrix} = \begin{bmatrix} \mathbf{A} - B_1 K_P & -B_1 K_E \\ LC - B_1 K_P & \mathbf{A} - B_1 K_E - LC \end{bmatrix} \begin{bmatrix} x \\ \hat{x} \end{bmatrix} + \begin{bmatrix} B_2 - B_1 K_P D_2 \\ 0 \end{bmatrix} U_2 \tag{9}$$

where K_P and K_E are the gain vectors associated with the plant and estimator states respectively. For the precision mode,

$$\begin{bmatrix} K_P \\ K_E \end{bmatrix} = \begin{bmatrix} k_1 & k_2 & 0 & 0 & 0 \\ 0 & 0 & k_3 & k_4 & k_5 \end{bmatrix}$$

The $B_1 K_P D_2$ term is included in Eq. (9) to maintain generality, even though the $K_P D_2$ product is always zero in the absence of plant acceleration feedback.

From Eq. (9), it is seen that Eq. (6) for the estimator error is also applicable to the precision mode case, and the steady-state estimator error $\tilde{x}$ is therefore identical in both the computer mode and precision mode. However, the altered form of the control gains K_P and K_E in the precision mode change the coupling of the integral position x_1 and its estimate $\hat{x}_1$. Accordingly, when solving Eq. (9) for final values, the row and column corresponding to the integral estimate $\hat{x}_1$ are deleted, and those corresponding to the integral x_1 are retained. As a result, the final value solution of Eq. (9) yields the expected zero value for the position x_2 and a nonzero position estimate $\hat{x}_2$. This result implies a nonzero estimator error $\tilde{x}$ consistent with Eq. (6).

These observations demonstrate an interesting duality between the two control modes, whereby the substitution of plant states for their corresponding estimator states in the control gain law results in the interchange of the final values of plant and estimated position variables. This tends to confirm the validity of the general expressions of Eqs. (7) and (9), and indicates that in the precision-control mode, a zero steady-state error always results from a disturbance torque input.

VII. Compliance Transient Properties

The shape of the transient response to disturbance torques can be inferred from the relative locations of the poles and zeros of the compliance transfer functions for the various system configurations. For the open-loop and hardware PID feedback systems, the poles and zeros are defined by Eqs. (2) and (3), respectively, where it is seen that the poles are the same as those associated with the respective command input-output transfer functions.

For the state variable controller configurations, the poles are the respective eigenvalues of the square system matrices in Eqs. (7) and (9). The corresponding zeros are the complex frequencies of zero response of $\dot{x}$, $\hat{\dot{x}}$, and Y for any disturbance input U_2 and initial condition. Thus, for the computer-mode configuration of Eq. (7), the response zeros are the roots of

$$\begin{bmatrix} (sI - \mathbf{A}) & -B_1 K & -B_2 \\ LC & (sI - \mathbf{A} + B_1 K + LC) & 0 \\ C & 0 & 0 \end{bmatrix} \begin{bmatrix} x \\ \hat{x} \\ U_2 \end{bmatrix} = \begin{bmatrix} 0 \\ 0 \\ 0 \end{bmatrix}$$

To avoid the longhand expansion of the above determinant, the zeros were determined by a numerical evaluation of the transfer function zeros of the system of Eq. (7) with coefficient values representative of the 70-m azimuth servo.

The results coincide precisely with the two nonzero real roots of the determinant

$$\begin{bmatrix} [sI - \mathbf{A}] & B_2 \\ C & 0 \end{bmatrix}$$

at $-D_H/C_H$ and $-P_2$ (the root at zero is absent), and with the five eigenvalues of $[\mathbf{A} - B_1K - LC]$. A numerical computation of the eigenvalues of the square matrix of Eq. (7) shows that the accompanying poles are the five eigenvalues of $[\mathbf{A} - B_1K]$ and the five eigenvalues of $[\mathbf{A} - LC]$.

For the precision-mode configuration of Eq. (9), the response zeros are the zeros of

$$\begin{bmatrix} [sI - \mathbf{A} + B_1K_P] & -B_1K_E & -B_2 \\ LC - B_1K_P & [\mathbf{sI} - \mathbf{A} + B_1K_E + LC] & 0 \\ C & 0 & 0 \end{bmatrix}$$

$$\times \begin{bmatrix} x \\ \hat{x} \\ U_2 \end{bmatrix} = \begin{bmatrix} 0 \\ 0 \\ 0 \end{bmatrix}$$

Numerical evaluation of the transfer function zeros indicates two real zeros at $-D_H/C_H$ and $-P_2$, two zeros at the origin (one of which is canceled by a pole), and four additional real and complex zeros which are near, but noncoincident with, four of the poles of the square matrix of Eq. (9). This result indicates that unlike the computer-mode case of Eq. (7), the precision mode exhibits zero steady-state disturbance torque compliance. In addition, the low-frequency zero from the eigenvalues of $[\mathbf{A} - B_1K - LC]$ arising from Eq. (7) is absent in this case, resulting in a faster disturbance recovery transient in the precision mode. The system poles computed from Eq. (9) are identical with those from Eq. (7) for the computer mode.

From the foregoing and from Eqs. (2) and (3), it is seen that the real zeros at $-D_H/C_H$ and $-P_2$ appear in the compliance expressions for the open-loop and PID feedback systems, as well as for the computer and precision-mode state variable controllers. The differing steady-state compliance properties of these four configurations arise from the presence of poles or zeros at the origin. This commonality implies that all four configurations exhibit identical disturbance transient characteristics for a short time interval following the transient. This in turn implies that the initial transient characteristics of the state variable controllers are governed solely by the plant parameters, and the departure from this initial characteristic is governed by the controller.

VIII. Numerical Results

Numerical evaluations of the differential equations incorporated the physical parameter values of Table 1, the control coefficients of Table 2, and the disturbance torque parameters of Table 3. Physical parameter values of Table 1 were derived from component specifications according to [1] with the rate loop gain and network parameters based on [4]. The K_R value of 5.107 corresponds to a rate loop dc gain product of 40. The values shown for damping D_H are calculated using Eq. (1) and correspond to the axis rate range of 1 to 40 times the sidereal rate with added leakage Q_{HL}. Aerodynamic parameters used in determining wind torques were extrapolated by McGinness[1] from earlier wind-tunnel tests performed on scale models of the 64-m antenna.

The position feedback control gain K and estimator gain L shown in Table 2 were calculated according to the optimal control criteria of Alvarez and Nickerson [5]. The baseline values L_1 and K_4 in the table were calculated to duplicate the dominant closed-loop poles of [5] when applied to the model of Fig. 3. Alternate parameter sets were calculated in a similar manner with weighting adjusted to shift the dominant poles inward or outward from the origin. Those estimator gains that include integral terms were calculated using an alternate output vector $H = [1 \quad 1 \quad 0 \quad 0 \quad 0]$, which included equal weighting of integral and position.

The wind torque moments in Table 3 were calculated according to McGinness[2] using the torque relationship

$$\text{torque} = \frac{C_T q \pi D_A^3}{4} \tag{10a}$$

where C_T is the aerodynamic lift coefficient, the dynamic wind pressure is

$$q = \frac{\rho v^2}{2} \tag{10b}$$

with air density, $\rho = 0.00238$ lb/ft^3, and wind velocity, v.

[1] H. McGinness, "Effects of Wind Loading on 64- And 72-Meter Diameter Antenna" (JPL internal report), Reorder No. 84-2, May 1984.

[2] McGinness, ibid.

From Eqs. (10a) and (10b), the disturbance torque is seen to be a quadratic function of the wind velocity, so the disturbance imparted by a step change in velocity depends on the initial and final velocities rather than the step amplitude. Thus, if v_m is the mean of the initial and final velocities and v_d is their difference, the torque disturbance is proportional to the product $v_m v_d$. The worst-case disturbance then results when a large step-velocity change is superposed on a large mean velocity such that their product is a maximum. Assuming 30 mph as the maximum average wind and 12 mph as the maximum gust, the worst-case disturbance corresponds to a step change between 24 and 36 mph.

Breakaway friction torque levels were extracted from acceptance-test data recorded when the overseas antennas were built in 1972. The range of values shown is consistent with more recent informal reports of observations at the Goldstone site.

The differential hydraulic pressures corresponding to the disturbance torques are included in Table 3. Because of its linear relationship to torque and its ease of direct measurement, the differential pressure has become a familiar unit of torque measurement to those working with the antenna.

The disturbance torque transient responses of the open-loop, computer-mode, and precision-mode configurations obtained from the time solutions of Eqs. (7) and (9) with $K = K_4$ and $L = L_1$ are shown in Fig. 5. The disturbance input corresponds to a 12-mph wind step combined with a 30-mph mean wind. The open-loop case was obtained from Eq. (7) with zero value of control gain K. The comparatively rapid recovery of the precision mode and the finite steady-state error of the computer mode are clearly visible in the time responses. The slower recovery of the computer mode is attributed to a low-frequency transfer function zero arising from Eq. (7), which is absent from the precision-mode case.

Figure 6 shows the computer-mode disturbance torque transient response for various antenna rates. The responses were generated from Eq. (7), where the D_H/C_H term in the **A** matrix was adjusted according to Eq. (1) for each antenna rate. The effect of the changing D_H/C_H zero in the transfer function is evident from the change of the transient shape and of the final value. Figure 6 can also be used to judge the effects of increased hydraulic leakage by converting a known volumetric leakage to an equivalent antenna rate through the hydraulic displacement and gear ratio. The characteristic corresponding to the sum of the leakage equivalent rate and actual rate then represents the system behavior.

Figure 7 shows the computer-mode transient response for the various values of control gain K listed in Table 2. As indicated earlier from the general properties of Eqs. (6) and (7), the gain K is seen to influence the speed of recovery, but has no effect on the final value.

Figure 8 shows the computer-mode transient response for the various values of estimator gain L listed in Table 2. The effect of those L vectors having finite integral error correction terms l_1 is seen in the faster recovery time, as well as reduction of the final value. The final value for those cases is still finite due to the absence of position integral feedback.

Figure 9 shows the precision-mode transient response for the various values of control gain K listed in Table 2. Increasing values of K are seen to decrease the peak error and speed the recovery transient.

Figure 10 shows the precision-mode transient response for the various values of estimator gain L listed in Table 2. As expected, the estimator gain L has little effect on the compliance transient when the response of the estimator is faster than that of the control gain.

IX. Summary and Conclusions

The transient disturbance-torque rejection properties of the 70-m axis servos are shown to be governed by physical hardware parameters, as well as by the properties of the software-control algorithm. In particular, the effective hydraulic damping D_H/C_H, which is strongly affected by hydraulic leakage as well as by axis rate, determines the peak transient error, and in the case of the computer mode it also produces a finite steady-state error. The peak and steady-state disturbance-torque errors are essentially unaffected by the control gain K, but can be reduced by increased estimator gain L at the expense of noise rejection.

The precision-control mode, by virtue of the direct feedback of hardware (as opposed to estimated) position and integral errors, is shown to have disturbance torque rejection properties superior to those of the computer mode. This deficiency of the computer mode results from the omission of the position integral error from the estimator equations, and can be corrected by modifying the equations to include the integral. Significant improvement can also be obtained by modifying the estimator gain parameter L to include a coefficient corresponding to the integral position estimate.

References

[1] R. E. Hill, "A New State Space Model for the NASA/JPL 70-Meter Antenna Servo Controls," *TDA Progress Report 42-91*, vol. July-September 1987, Jet Propulsion Laboratory, Pasadena, California, pp. 247–264, November 15, 1987.

[2] R. E. Hill, "A New Method for Analysis of Limit Cycle Behavior of the NASA/JPL 70-Meter Antenna Axis Servos," *TDA Progress Report 42-97*, vol. January–March 1989, Jet Propulsion Laboratory, Pasadena, California, pp. 98-111, May 15, 1989.

[3] C. D. Johnson, "Disturbance Accommodating Control: A History of Its Development," *Recent Advances in Engineering Science: Proc. 15th Annual Meeting Soc. of Eng. Science*, R. L. Sierakowski, editor, pp. 331–336, 1978.

[4] R. E. Hill, "Dynamic Models for Simulation of the 70-Meter Antenna Axis Servos," *TDA Progress Report 42-95*, vol. July–September 1988, Jet Propulsion Laboratory, Pasadena, California, pp. 32–50, November 15, 1988.

[5] L. S. Alvarez and J. Nickerson, "Application of Optimal Control Theory to the Design of the NASA/JPL 70-Meter Antenna Axis Servos," *TDA Progress Report 42-97*, vol. January–March 1989, Jet Propulsion Laboratory, Pasadena, California, pp. 112–126, May 15, 1989.

Table 1. The 70-m antenna axis servo parameter values

Symbol	Parameter	Units	Value
J_{MA}	Inertia moment, azimuth	in.-lb-sec	12.0
J_{ME}	Inertia moment, elevation	in.-lb-sec	8.0
V_H	Hydraulic displacement	$in.^3$/radian	1.53
C_H	Hydraulic compressibility	$in.^3$/psi	0.00314
D_H	Hydraulic damping	$in.^3$/psi-sec	0.00188 to 0.0754
Q_{HL}	Hydraulic leakage	$in.^3$/sec	1.67
N	Reduction gear ratio	dimensionless	28730
P_1	Tach network negative pole frequency	sec^{-1}	80
P_2	Lag network negative pole frequency	sec^{-1}	0.24
Z_1	Tach network negative zero frequency	sec^{-1}	5.0
Z_2	Lag network negative zero frequency	sec^{-1}	4.4
K_R	Rate loop gain constant	$in.^6$	5.11
K_V	Valve flow constant	$in.^3$/mA-sec/$psi^{0.5}$	0.731
P_V	Valve pressure drop	psi	2750
C_{TA}	Aerodynamic lift coefficient, azimuth	dimensionless	0.1217
C_{TE}	Aerodynamic lift coefficient, elevation	dimensionless	0.1231
D_A	Reflector aerodynamic diameter	m	70

Table 2. System, control gain, and estimator parameters

(a) System matrices

$$\mathbf{A} = \begin{bmatrix} 0 & 1.0000 & 0 & 0 & 0 \\ 0 & 0 & 1.0000 & 0 & 0 \\ 0 & 0 & 0 & 8.3333 & 0 \\ 0 & 0 & -23.7194 & -27.7072 & 13.2484 \\ 0 & 0 & -5.1070 & -8.5117 & -0.2400 \end{bmatrix}$$

$$\mathbf{B} = \begin{bmatrix} 0 & 0 \\ 0 & 0 \\ 0 & 0.0833 \\ 16.2643 & -0.2711 \\ 5.1070 & -0.0851 \end{bmatrix}$$

$$\mathbf{C} = \begin{bmatrix} 0 & 1.0000 & 0 & 0 & 0 \end{bmatrix}$$

$$\mathbf{D} = \begin{bmatrix} 0 \end{bmatrix}$$

(b) Control gains K

Control gain K	Numerical value	Control poles from eigenvalue $(\mathbf{A} - BK)$
K_1	0.5200	$-12.2372 + 12.5297i$
	1.3417	$-12.2372 - 12.5297i$
	0.5712	-2.5455
	0	$-0.4636 + 0.4268i$
	0	$-0.4636 - 0.4268i$
K_2	0.3162	$-12.8664 + 9.5595i$
	0.9097	$-12.8664 - 9.5595i$
	0.1685	-2.4141
	0.0162	$-0.3937 + 0.3861i$
	0.1416	$-0.3937 - 0.3861i$
K_3	0.4472	$-12.9520 + 9.4886i$
	1.1113	$-12.9520 - 9.4886i$
	0.2087	-2.4404
	0.0279	$-0.4668 + 0.4539i$
	0.1716	$-0.4668 - 0.4539i$
K_4	0.6325	$-13.1214 + 9.3446i$
	1.3684	$-13.1214 - 9.3446i$
	0.2642	-2.4911
	0.0500	$-0.5509 + 0.5291i$
	0.2106	$-0.5509 - 0.5291i$
K_5	0.8944	$-13.4526 + 9.0474i$
	1.7032	$-13.4526 - 9.0474i$
	0.3450	$-0.6445 + 0.6078i$
	0.0916	$-0.6445 - 0.6078i$
	0.2629	-2.5861
K_6	1.2649	$-14.0877 + 8.4129i$
	2.1515	$-14.0877 - 8.4129i$
	0.4690	$-0.7426 + 0.6822i$
	0.1699	$-0.7426 - 0.6822i$
	0.3339	-2.7556

Table 2. System, control gain, and estimator parameters (contd)

(c) Estimator gains

Estimator gain L	Numerical value	Estimator poles from eigenvalue $(\mathbf{A} - BK_4 - LC)$	Compliance zeros from eigenvalue $(\mathbf{A} - BK_4 - LC)$
L_1	0	$-12.7800 + 9.6298i$	$-13.1060 + 9.3382i$
	0.4546	$-12.7800 - 9.6298i$	$-13.1060 - 9.3382i$
	0.0033	-2.3859	-2.1842
	-0.0020	-0.4559	-1.4267
	0.0026	0	-0.4674
L_2	0.8638	$-12.4988 + 9.7652i$	$-12.6999 + 9.4375i$
	3.1261	$-12.4988 - 9.7652i$	$-12.6999 - 9.4375i$
	4.8336	-4.8845	-5.0267
	-7.6308	-1.1912	-2.5190
	-9.1392	0	-0.0162
L_3	0.8075	$-12.7656 + 9.6345i$	$-13.0283 + 9.3205i$
	1.4625	$-12.7656 - 9.6345i$	$-13.0283 - 9.3205i$
	1.1140	$-1.9392 + 0.7044i$	$-2.6041 + 1.3095i$
	-0.6472	$-1.9392 - 0.7044i$	$-2.6041 - 1.3095i$
	0.5716	0	-0.0333
L_4	0.6204	$-12.7686 + 9.6345i$	$-13.0829 + 9.3379i$
	0.5545	$-12.7686 - 9.6345i$	$-13.0829 - 9.3379i$
	0.1357	-2.5083	$-2.0488 + 0.4207i$
	-0.3804	-0.4562	$-2.0488 - 0.4207i$
	-0.5582	0	-0.1267

Table 3. Typical disturbance torque levels

	Azimuth	Elevation
Wind moments for 30-mph wind	2.67×10^6 ft-lbs 729 psi	2.70×10^6 ft-lbs 738 psi
Breakaway friction torque	$1.03 - 1.28 \times 10^6$ 280 – 350 psi	$0.84 - 1.46 \times 10^6$ ft-lbs 230 – 400 psi

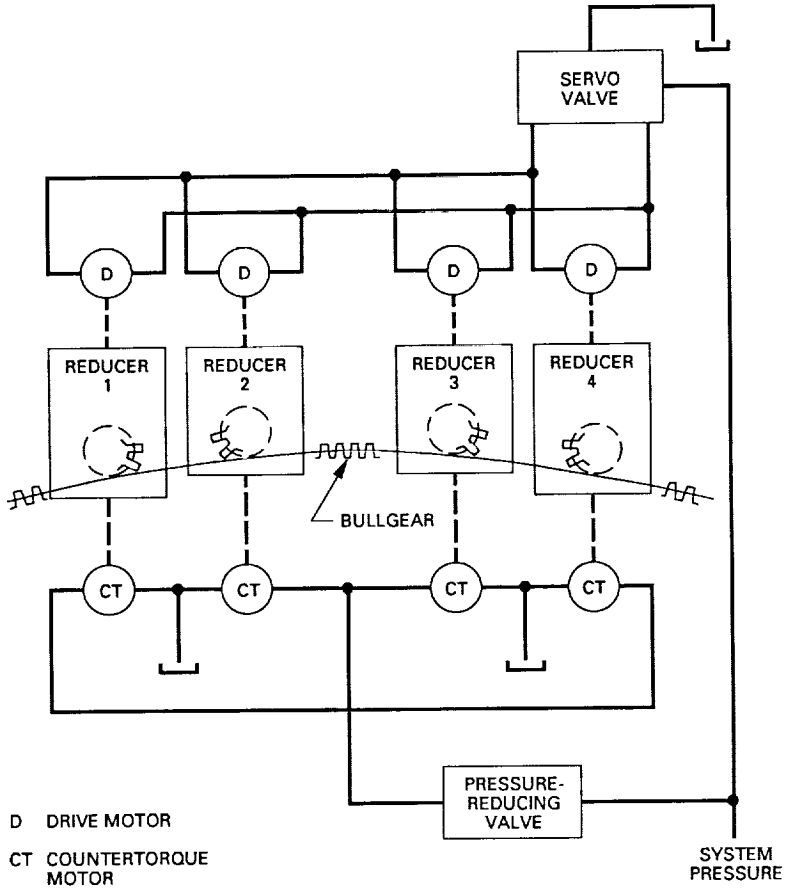

Fig. 1. The 70-m antenna axis servo countertorque system.

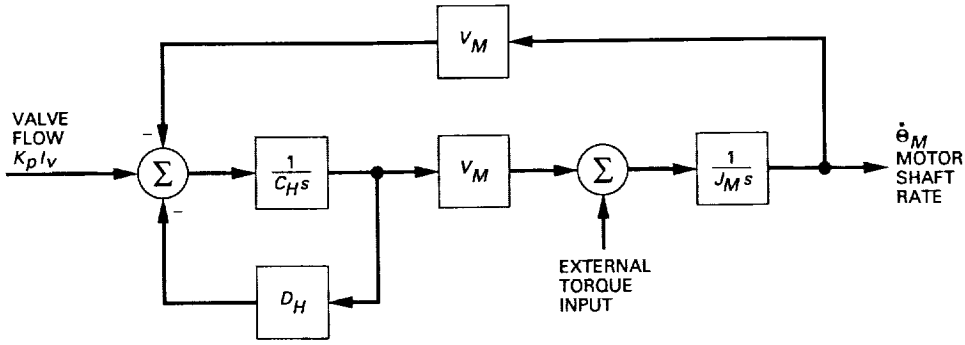

Fig. 2. Servo hydromechanical system linearized model.

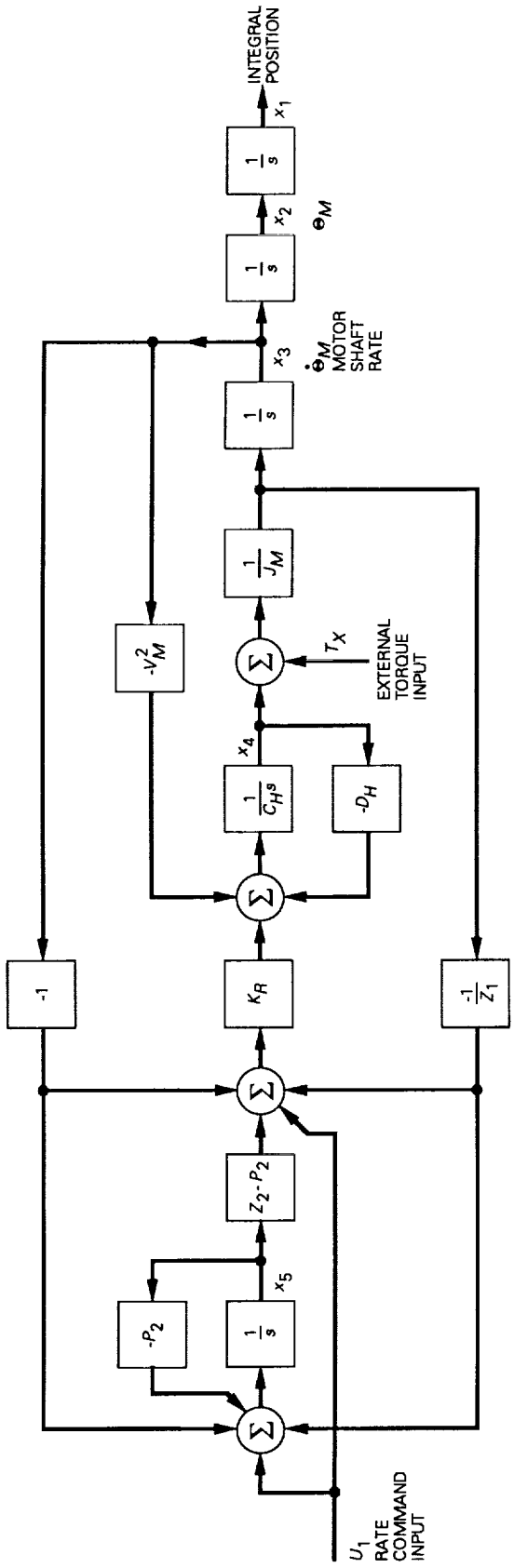

Fig. 3. Servo condensed plant block diagram.

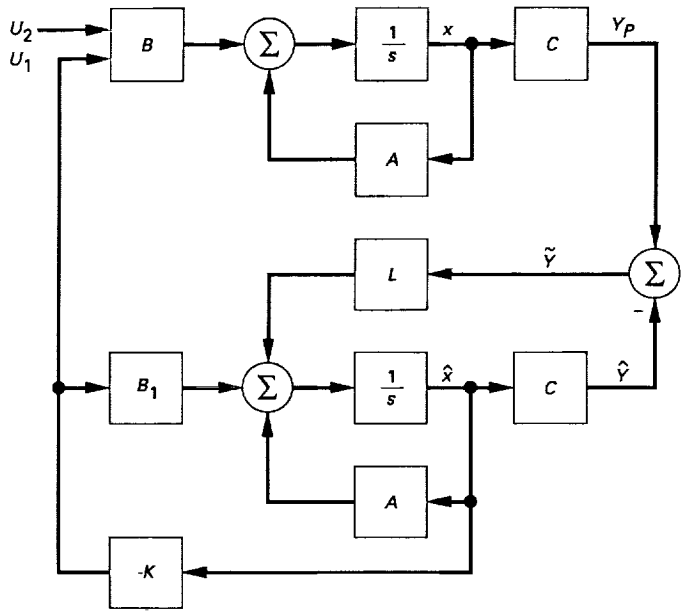

Fig. 4. Servo position controller block diagram.

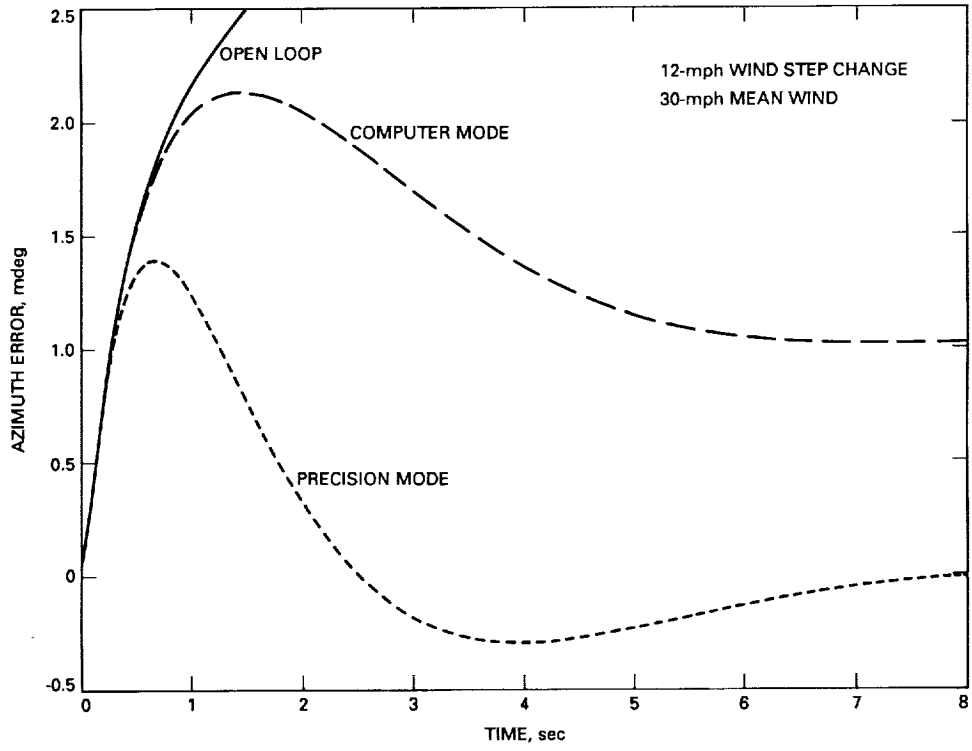

Fig. 5. Disturbance torque transient response of open-loop, computer-mode, and precision-mode configurations.

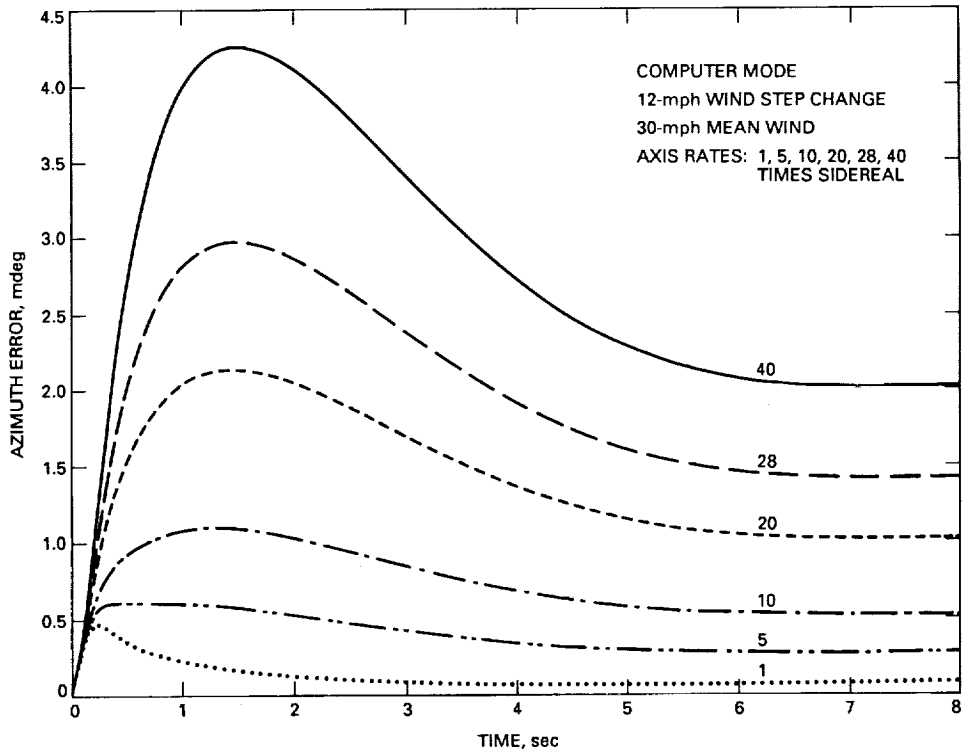

Fig. 6. Disturbance torque transient response for various axis rates.

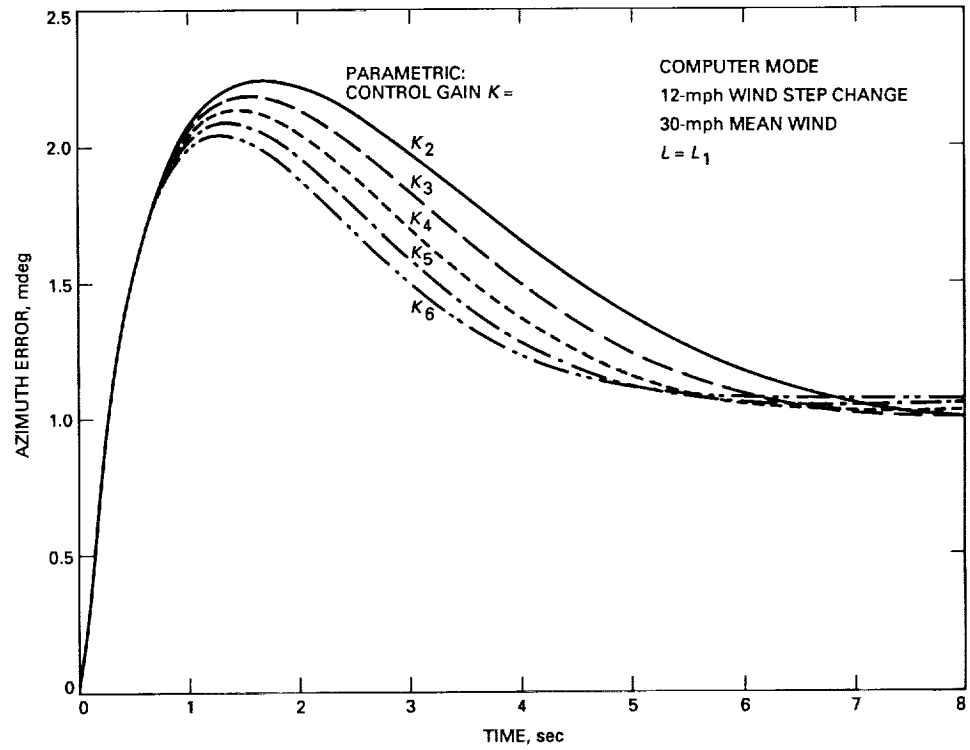

Fig. 7. Computer-mode disturbance torque transient response for various *K*.

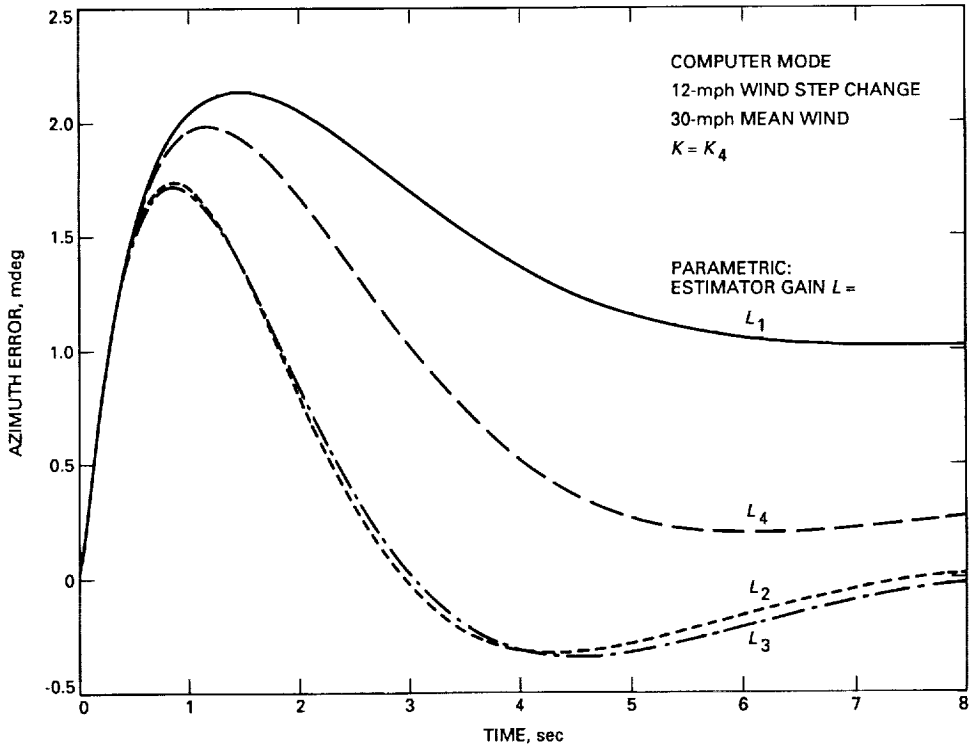

Fig. 8. Computer-mode disturbance torque transient response for various L.

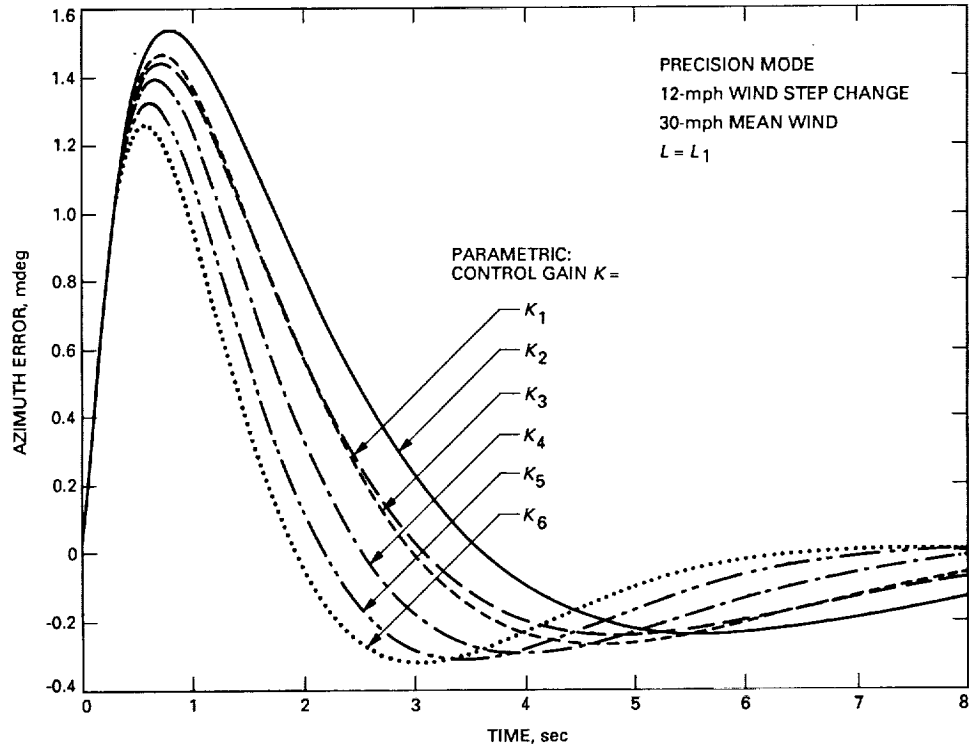

Fig. 9. Precision-mode disturbance torque transient response for various K.

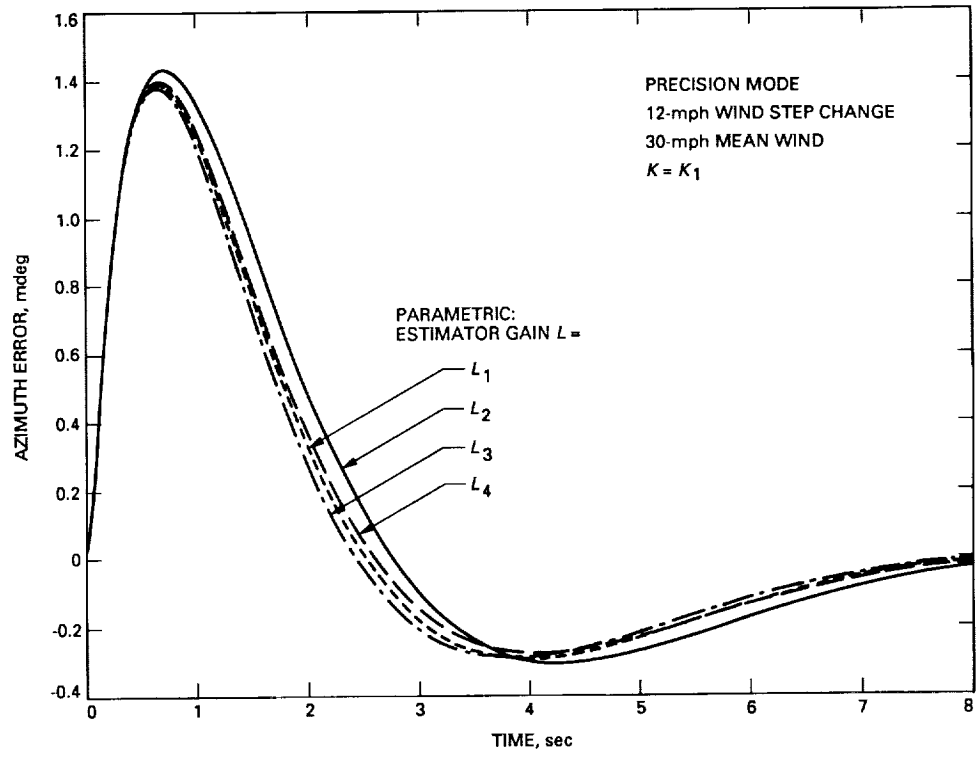

Fig. 10. Precision-mode disturbance torque transient response for various L.